Journal of Statistical Physics, Vol. 50, Nos. 3/4, 1988

Passive Scalars, Three-Dimensional Volume-Preserving Maps, and Chaos

Mario Feingold,[1] Leo P. Kadanoff,[1] and Oreste Piro[1,2]

Received October 21, 1987

The dynamics of a medium-sized particle (passive scalar) suspended in a general time-periodic incompressible fluid flow can be described by three-dimensional volume-preserving maps. In this paper, these maps are studied in limiting cases in which some of the variables change very little in each iteration and others change quite a lot. The former are called slow variables or actions, the latter fast variables or angles. The maps are classified by their number of actions. For maps with only one action we find strong evidence for the existence of invariant surfaces that survive the nonlinear perturbation in a KAM-like way. On the other hand, for the two-action case the motion is confined to invariant lines that break for arbitrary small size of the nonlinearity. Instead, we find that adiabatic invariant surfaces emerge and typically intersect the resonance sheet of the fast motion. At these intersections surfaces are locally broken and transitions from one to another can occur. We call this process, which is analogous to Arnold diffusion, singularity-induced diffusion. It is characteristic of two-action maps. In one-action maps, this diffusion is blocked by KAM-like surfaces.

KEY WORDS: Incompressible fluid; passive scalars; three-dimensional volume-preserving maps; action–angle variables; Arnold diffusion; invariant structures.

1. INTRODUCTION

Various metal powders (e.g., aluminum) are frequently used for flow visualization in hydrodynamic systems.[1] Those powders are composed of tiny particles, which are driven by the velocity field of the flow $\mathbf{u}(x, y, z, t)$. Therefore, the position $\mathbf{r}(t) = (x(t), y(t), z(t))$ of the powder particles satisfies

$$\dot{\mathbf{r}} = \mathbf{u} \tag{1.1}$$

[1] James Franck Institute, University of Chicago, Chicago, Illinois 60637.

[2] On leave of absence from the Departamento de Física, Universidad Nacional de La Plata, (1900), La Plata, Argentina.

0022-4715/88/0200-0529$06.00/0

with different initial conditions for different particles. Ideally, the powder particles are small enough such that they do not perturb the velocity field $\mathbf{u}$, but also big enough not to be undergoing a Brownian diffusive motion as a result of colliding with the fluid molecules. The abstract particles satisfying both requirements are useful idealization in fluid mechanics and are known in the literature as passive scalars (PS). Some local properties such as temperature or the density of a second fluid can be regarded under some conditions as PS. Therefore, the understanding of the dynamics of PS is important in the theory of mixing of fluids, which in turn has a fundamental role in fields like combustion and chemical reactions.

For steady flows, the trajectories of the passive scalars given by Eq. (1.1) are nothing but the streamlines of the velocity field. Some nonturbulent flow fields $\mathbf{u}$ lead to orderly streamlines, but in other cases even very simple nonturbulent flows can produce chaotic streamlines. The PS is then said to display "Lagrangian turbulence" as opposed to "Eulerian turbulence," which implies chaotic behavior in $\mathbf{u}$ itself.

The issue of the topology of streamlines in 3D, incompressible, steady, ideal fluid flows was first addressed by Arnold.[2] He proved that if the vorticity $\boldsymbol{\omega}$ ($\boldsymbol{\omega} = \nabla \times \mathbf{u}$) and the velocity are nowhere parallel, then Eq. (1.1) is integrable. That means that almost all possible PS trajectories (streamlines) lie on 2-tori. At the opposite extreme, the *ABC* flow

$$\begin{aligned} \dot{x} &= u_x = A \sin z + C \cos y \pmod{2\pi} \\ \dot{y} &= u_y = B \sin x + A \cos z \pmod{2\pi} \\ \dot{z} &= u_z = C \sin y + B \cos x \pmod{2\pi} \end{aligned} \tag{1.2}$$

which satisfies the Beltrami property $\omega = \lambda \mathbf{u}$ with $\lambda = 1$, was suggested by Arnold as an example of a most nonintegrable case. Extensive studies of the *ABC* model have shown the coexistence of chaotic trajectories and KAM-like surfaces at various values of parameters.[3] From the fluid dynamical viewpoint, $\mathbf{u}_{ABC}$ is a solution of the Euler equation.[3] *Arnold has conjectured*[3] *that the way to Eulerian turbulence is facilitated by the preexistence of Lagrangian turbulence as opposed to regular streamlines.*

[3] If a forcing term

$$\mathbf{f} = \nu(A \sin z + C \cos y, B \sin x + A \cos z, C \sin y + B \cos x)$$

is introduced, then $\mathbf{u}_{ABC}$ is a solution of the Navier–Stokes equation as well,

$$\partial_t \mathbf{u} + \mathbf{u} \cdot \nabla \mathbf{u} = -\nabla p + \nu \nabla^2 \mathbf{u} + \mathbf{f}$$
$$\nabla \cdot \mathbf{u} = 0$$

Moreover, it has been recently shown[4] that for large viscosity ν, $\mathbf{u}_{ABC}$ is the only stable solution of the Navier–Stokes equation. As the viscosity ν is lowered, a sequence of bifurcations is triggered, which eventually leads to Eulerian turbulence.

On the other hand, the influence of chaotic motion of passive scalars on stirring and fluid mixing has been recently investigated in two-dimensional, time-dependent flows.[5] Aref has stressed that for 2D flows the motion of PS in the real space is equivalent to the Hamiltonian dynamics of a phase space point. In fact, if Ψ is the stream function, then

$$\dot{x} = -\partial\Psi/\partial y; \qquad \dot{y} = \partial\Psi/\partial x \tag{1.3}$$

Renaming the variables $(x, y, \Psi) \to (p, x, H)$ in Eq. (1.3), we obtain the usual Hamilton equations for a one-degree-of-freedom system. Therefore, autonomous 2D flows are integrable and mixing in these systems is highly inefficient. When time dependence is added to the stream function, PS typically undergo the same kind of chaotic motion arising in nonautonomous Hamiltonian systems and the transport is strongly enhanced. This enhancement of transport is known as chaotic advection and was investigated both numerically[6] and experimentally.[7] For example, Gollub and Solomon[7] have analyzed 2D flows in the Raleigh–Benard system as they are modified by the onset of oscillation in the velocity field. They found that when the longitudinal rolls start to oscillate, the effective PS diffusion constant suddenly grows by more than one order of magnitude.

Both autonomous and nonautonomous Hamiltonian systems induce volume-preserving flows in phase spaces (Liouville theorem). These phase spaces, of course, have an even dimensionality. In contrast, incompressible flows (like the *ABC* model, for example) satisfy

$$\nabla \cdot \mathbf{u} = 0 \tag{1.4}$$

and hence preserve instead volumes in the usual *three-dimensional* space. When the flow is two-dimensional, the problem simplifies to one that can be studied by Hamiltonian methods. Thus, the Aref and Gollub–Solomon examples are in the same category as 2D area-preserving maps, which have been extensively studied.[8,9] The same is true to some extent for the *ABC* flow, because special choices of the surface of section can assure the local invariance of the areas. In this paper, we study the essentially three-dimensional problems that can arise when a flow of the form (1.1) is periodic in time. In this case, the flow can be represented by a Poincaré or stroboscopic map that is three-dimensional and volume-preserving. In some sense, these maps lie between $N = 2$ and $N = 3$ Hamiltonian systems. It is well known for N-degree-of-freedom Hamiltonians that regular motion is confined to N-tori. For $N = 2$ Hamiltonians, the 2-tori of regular motion divide the 3D energy surface into an inside part and an outside one.

Therefore, as long as a regular 2-torus exists, chaotic motion is bounded to either its outside or its inside, depending on the initial condition. As the size ε of the nonlinearity is increased, phase space will become connected only after the last 2-torus breakdown.[10] Even then, small portions of phase space (islands) remain isolated. However, their relative size decreases as we enter deeper into the chaotic regime. In the $N=3$ case, on the other hand, the 3-tori cannot separate the 5D energy surface, and phase space is always connected. Diffusive motion for $N \geqslant 3$ is possible for arbitrarily small ε. This phenomenon is known as Arnold diffusion.[11] A qualitative continuity is still maintained with the $N=2$ case, since for small ε the tori form dense bundles, which make diffusion very slow. Actually, it has been shown that $D \propto \exp(-1/\varepsilon^{1/2})$,[8,9,11] where D is the diffusion constant. While the $N=2$ case has been thoroughly investigated, very little is known about $N \geqslant 3$ Hamiltonian problems. This is partly because of the difficulties in visualizing trajectories generated by 4D maps.

Thus, we have two reasons for our interest in 3D volume-preserving maps. On one side the possible enhancement of the diffusive properties is important from the fluid dynamical point of view. Going from steady to time-periodic velocity fields also implies an increase in the Reynolds number and therefore a step closer to the extremely hard problem of turbulence.[12] On the other hand, 3D maps represent intermediate cases between two qualitatively different behaviors. While they might display phenomena unknown in $N=2$ Hamiltonians, their analysis should be simpler than the $N=3$ case. However, the absence of the canonical structure in odd dimensions makes inapplicable most of the general results of the Hamiltonian theory. Very little qualitative information on the behavior of 3D volume-preserving maps is available in the literature.[13]

To study the qualitative properties of 3D volume-preserving maps, we follow in the footsteps of KAM and imagine perturbations about simplified models in which some variables (actions) are unchanged from iteration to iteration and others (angles) change in each iteration. A small perturbation makes the actions vary slowly. We then ask about the structure of invariant sets in the small-perturbation case.

Naturally, one distinguishes between two cases: maps with two actions and maps that have but one. The action variables are the constants of motion in the integrable limit of these maps. We might expect the emerging invariant structures to have the same codimension as the number of actions involved. The restriction of the maps to any of their invariant objects is a uniform rotation of each angular (fast) variable. The frequencies of these rotations are determined by the values of the actions labeling the given invariant object. Whenever an integer linear combination of the angular frequencies is commensurate with 2π we refer to the trajectory as resonant.

Maps with only one action will be found to display invariant surfaces. These are preserved under small nonlinear perturbations in a similar manner to KAM tori in Hamiltonian systems. Since the frequencies of the two angular motions $\omega_1(I)$ and $\omega_2(I)$ are just functions of the unique action, they should be constant along a given invariant surface. In this case the condition for resonance can be written as

$$m\omega_1(I) + n\omega_2(I) = 2\pi k \tag{1.5}$$

where m, n, and k are arbitrary integers. The surfaces on which Eq. (1.5) is satisfied break and layers of chaotic motion emerge instead. These layers will be bounded by the intact invariant surfaces. As a consequence, single trajectories cannot diffuse throughout the available space.

On the other hand, when there are two conserved action variables the invariant surfaces are lines. These do not separate the space. Hence, when one turns on a small perturbation one might expect to find Arnold-like diffusion through bundles of invariant lines. In fact, we do find unbounded diffusive motion, but engendered by a different mechanism. To our surprise, we find that almost all invariant lines break under arbitrarily small perturbations and are adiabatically replaced by invariant surfaces. We will show, however, that the frequency of the angular motion varies over the invariant surfaces. Moreover, the angular resonances are defined in this case by the equation

$$n\omega(I_1, I_2) = 2\pi k \tag{1.6}$$

where I_1 and I_2 are the actions and m and k are arbitrary integers. In contrast with the one-action case, the resonance sheets defined in (1.6) typically intersect a continuous set of adiabatically invariant surfaces. A *local* breakdown of the invariant surfaces occurs at the intersections, while the remaining part of the surface survives at a given order of the perturbation expansion. Surfaces are connected to each other through the resonances, allowing trajectories to diffuse over all space.

The extreme cases of three-action maps or three-angle ones are less interesting. For the former, the conservation requirement for three variables implies that the integrable case is the identity map (every point of the space is invariant). Small perturbations of the identity are actually flows instead of maps and this behavior has been studied before.[3] In turn, three-angle maps do not display any invariant structure of dimension less than three and generically chaotic behavior is expected. Finally, we will conclude that the dynamics of 3D maps is governed by both chaotic trajectories and invariant surfaces, while the invariant lines are responsible of the global ordering of the space.

The paper is organized as follows. In Section 2 the general framework of 3D volume-preserving maps is presented. We then derive our models and analyze their integrable limits, fixed points, and cycles. We end the section with a discussion on some special properties of Liapunov numbers for reversible 3D maps. In Section 3 numerical and perturbative methods are used to describe both the KAM-like behavior of nearly integrable one-action maps and the existence of diffusive motion at arbitrarily small nonlinearities in the two-action case. In Section 4 we discuss and summarize our findings.

2. GENERAL PROPERTIES OF 3D MAPS

The standard map

$$I' = I + K \sin \theta, \qquad \theta' = \theta + I' \tag{2.1}$$

which can be derived from the Hamiltonian of a periodically kicked rotor, is usually considered a representative of 2D area-preserving maps. For small values of the nonlinearity parameter K, it can be described by saying that it has an action variable that is characterized by a zero average variation and an angle variable with the frequency determined by the action. In the integrable limit given by $K = 0$ the motion consists of angular rotation on invariant lines labeled by the action, which is fixed. For small K, the variation in I is bounded, while that in θ is "linear." When considering 3D maps, the missing canonical structure obscures the difference between angle and action variables. However, we will pursue the action–angle classification to these maps following the guidelines suggested by the case of the standard map. We will consider as *action-like* those variables that label the invariant structures of the integrable cases. The angles are the variables parametrizing the motion on the invariant objects, and their associated frequencies are determined by the actions. Close to integrability, the actions are the slowly varying variables, while the angles are the fast ones. Of course, the nature of our variables changes as we pass from one region in parameter space to another. This reflects the lack of canonical structure in our problem.

A general form for 3D volume-preserving maps that are continuous perturbations of the identity recently has been derived by Thyagaraja and Haas.[14] Instead of following the general case, we will concentrate on maps of the form

$$\begin{aligned} x' &= x + F(x, z) \\ y' &= y + G(x', z) \\ z' &= z + H(x', y') \end{aligned} \tag{2.2}$$

which are clearly volume-preserving and, we believe, capture the main features of general 3D maps. They also have the advantage of being related to the flows defined by $\mathbf{u} = (F, G, H)$ through a naive discretization procedure, which involves the strobing of certain time-dependent flows. We will further illustrate this point in the examples. Since we will choose to confine the dynamics of the maps to a 3-torus, the continuity of the F, G, and H functions in Eq. (2.2) implies that these are periodic in each of their variables. Thus, the simplest nontrivial form of F, G, and H can be obtained by retaining only the lowest order terms of their Fourier expansion. In the following we will focus on the specific class of maps T defined by

$$\begin{aligned} x' &= x + A_1 \sin z + C_2 \cos y \pmod{2\pi} \\ y' &= y + B_1 \sin x' + A_2 \cos z \pmod{2\pi} \\ z' &= z + C_1 f(y') + B_2 g(x') \pmod{2\pi} \end{aligned} \tag{2.3}$$

where the f and g functions will be either sin or cos.

2.1. Integrable Cases and Invariant Objects

The trajectories of maps in three dimensions can belong to the following four categories:

1. *Fixed Points and Cycles.* As is well known from lower dimensional maps, these are solutions of $T^n(\mathbf{r}) = \mathbf{r}$. For volume-preserving 3D maps, fixed points and cycles are generically unstable.
2. *Invariant Curves.* A curve $\mathbf{r} = \mathbf{r}(t)$ embedded in a 3D space is invariant under the map T if for any point on the curve

$$\mathbf{r}(t') = T[\mathbf{r}(t)] \tag{2.4}$$

   Invariant curves of T^n that are not invariant under T^i, where $i = 1, \ldots, n-1$, are natural generalizations of n-cycles. We shall argue that invariant curves play a role in 3D analogous to cycles and fixed points in 2D.
3. *Invariant Surfaces.* Similarly, a surface $\mathbf{r} = \mathbf{r}(t, s)$ will be invariant if an arbitrary point on it satisfies

$$\mathbf{r}(t', s') = T[\mathbf{r}(t, s)] \tag{2.5}$$

   Like the invariant curve in 2D, the invariant surface in 3D serves to split the space into different regions which cannot connect with one another. Hence, they are crucial in setting the topology of all invariant sets.

4. *Chaotic Trajectories.* These are basically 3D objects which are either bounded between invariant surfaces or fill the whole periodicity box. Moreover, the Liapunov number for chaotic trajectories will be positive.

Using the map (2.3), we can now illustrate the classification of the variables given at the beginning of the section. If, for example, all the parameters are small ($\varepsilon \ll 1$), we obtain a *three-action map* (type T_{III}), which is close to the identity. With a proper rescaling of parameters and time, the behavior of this case will be similar to the flow obtained in the $\varepsilon \to 0$ limit.

Next, when all the parameters are small except for those in one of the equations of (2.3), a *two-action map* (type T_{II}) is obtained. For example, whenever A_1, B_1, C_2, A_2 are $O(\varepsilon)$, while C_1 and B_2 are of order unity, x and y play the role of actions, while z will be the angle. If $\varepsilon = 0$, x and y label the invariant lines along the z direction on which the integrable motion takes place.

In the third case, namely when all four parameters responsible for advancing a pair of variables (angles) are big (of order unity) and the other two are $O(\varepsilon)$, the T maps belong to the *one-action class* (type T_I). Nevertheless, since we are mainly concerned with the nearly integrable maps, we will also require the coupling between the angles to be small. Suppose, for instance, that A_1 and A_2 are the only big parameters; then x and y are angles, while z is an action.

Finally, whenever all parameters are big, a *three-angle map* (type T_0) is obtained which will generically display chaotic trajectories.

2.2. The *ABC* Map. An Example

Taking advantage of the existing knowledge on the ABC flow, we will employ in the following its discretized version, T_{ABC}, to illustrate the properties of 3D maps. T_{ABC} can be obtained by setting $A_1 = A_2 = A$, $B_1 = B_2 = B$, $C_1 = C_2 = C$, $f = \sin y$, and $g = \cos x$ in Eq. (2.3). It can also be derived from an ABC flow which in addition is time-periodically forced with delta functions

$$\begin{aligned} \dot{x} &= (A \sin z + C \cos y) \sum_{n=-\infty}^{\infty} \delta(t - n + \tau_1) \\ \dot{y} &= (B \sin x + A \cos z) \sum_{n=-\infty}^{\infty} \delta(t - n + \tau_2) \\ \dot{z} &= (C \sin y + B \cos x) \sum_{n=-\infty}^{\infty} \delta(t - n + \tau_3) \end{aligned} \tag{2.6}$$

where $0 < \tau_1 < \tau_2 < \tau_3 < 1$. From integrating (2.6) we obtain the ABC map T_{ABC},

$$\begin{aligned} x' &= x + A \sin z + C \cos y \pmod{2\pi} \\ y' &= y + B \sin x' + A \cos z \pmod{2\pi} \\ z' &= z + C \sin y' + B \cos x' \pmod{2\pi} \end{aligned} \tag{2.7}$$

Notice that T_{ABC} is a representative of the one-action maps whenever two of the parameters are small. Moreover, if those parameters vanish, T_{ABC} becomes integrable. For example, let us consider $T_A \equiv T_{ABC}$ $(B = C = 0)$

$$x' = x + A \sin z = x + 2\pi\rho_1 \pmod{2\pi} \tag{2.8a}$$

$$y' = y + A \cos z = y + 2\pi\rho_2 \pmod{2\pi} \tag{2.8b}$$

The motion for T_A is restricted to planes where the action variable z is constant. The value of the action variable determines the nature of this planar motion via the number-theoretic properties of the rotation numbers ρ_1 and ρ_2. The one-action resonance condition of Eq. (1.5) can be expressed in terms of ρ_1 and ρ_2 as

$$m\rho_1 + n\rho_2 = k \tag{2.9}$$

One can then distinguish three cases:

1. If one cannot find any integers m, n, and k satisfying Eq. (2.9), the trajectories of T_A densely fill entire $z = z_0$ planes. The nonresonant invariant planes will be shown to persist under small perturbations changing into invariant surfaces (see Section 2.1).
2. On planes $z = z_0$ where the resonance condition is satisfied, individual trajectories will only fill lines instead of the whole plane. In terms of the x, y variables the slope of this lines is m/n, where m and n are the integers that solve Eq. (2.9). For the integrable map T_A, each initial condition on a given resonant plane belongs to one of those lines. When nonlinearly perturbed, the resonant planes disintegrate. Most of its invariant lines disappear, except for a finite set. Numerically, we will find that half of the remaining lines are stable and half unstable. This is a scenario analogous to the one described by the Poincaré–Birkoff theorem in two-dimensional maps.
3. Whenever both $\rho_1 = p_1/q_1$ and $\rho_2 = p_2/q_2$ are rational, the trajectory is a cycle of period equal to the least common multiple of q_1 and q_2.

The first two types of trajectories will be analyzed in the next section. While for each value of A in T_A the invariant lines and planes are dense in the periodicity box, the cycles are extremely rare. In order to find a specific cycle, $\rho_i = p_i/q_i$, where $i = 1, 2$, A has to satisfy

$$A^2 = 4\pi^2(p_1^2/q_1^2 + p_2^2/q_2^2) \tag{2.10}$$

Equation (2.10) specifies in general a set S of measure zero such that if $A_i \in S$, one of these cycles can be found somewhere in the periodicity box. In principle, degeneracies such that two or more cycles will show up at the same value of A are possible. However, these are hard to predict, since that would be equivalent to solving an extension of the Euler problem over the rationals.

Before we pursue any further our analysis of cycles, it should be stressed that volume-preserving 3D maps have in general only linearly unstable ones. Volume preservation implies that each of the three eigenvalues of the Jacobian v_1, v_2, v_3 satisfies

$$v^3 + av^2 + bv - 1 = 0 \tag{2.11}$$

where $v_1 v_2 v_3 = 1$. Since the coefficients a and b are real, the solutions to Eq. (2.11) can be either all real or one real and the other two complex conjugates. Therefore, generically the moduli of the eigenvalues is different from one.

The fixed points of T_A are at $A = 2\pi l$, where $l = 0, 1, \ldots$. For $\rho_1 = \rho_2 = \rho_3 = 0$ we can easily find the fixed points of T_{ABC} as well. These satisfy

$$\begin{aligned} -A \sin z &= C \cos y = \pm[\tfrac{1}{2}(C^2 + A^2 - B^2)]^{1/2} \\ -B \sin x &= A \cos z = \pm[\tfrac{1}{2}(A^2 + B^2 - C^2)]^{1/2} \\ -C \sin y &= B \cos x = \pm[\tfrac{1}{2}(B^2 + C^2 - A^2)]^{1/2} \end{aligned} \tag{2.12}$$

There are eight of them and they exist only as long as the square roots in (2.12) are real. Therefore, solutions to (2.12) exist only outside the three right-angled cones centered on the axes of the (A, B, C) parameter space (see Fig. 1). On the surface of the cones, pairs of fixed points coalesce and disappear through a bifurcation mechanism similar to the saddle-node collision. The way in which the fixed points pair up depends on the cone on which they collide. For example, if this happens on the cone around the A axis, then Eqs. (2.12) become

$$\begin{aligned} -(C^2 + B^2)^{1/2} \sin z &= C \cos y = \pm C \\ -B \sin x &= (C^2 + B^2)^{1/2} \cos z = \pm B \\ -C \sin y &= B \cos x = 0 \end{aligned} \tag{2.13}$$

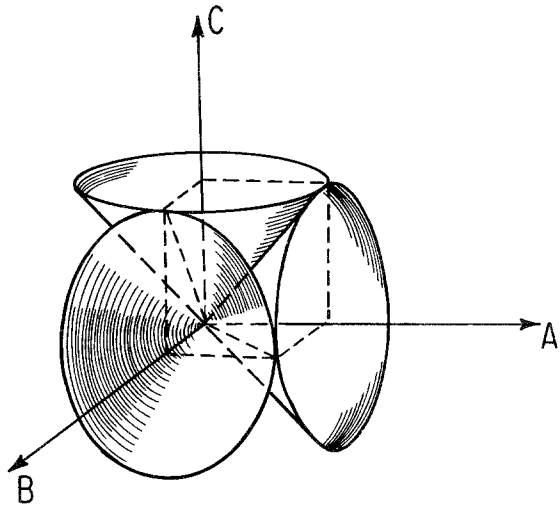

Fig. 1. The fixed points of type $\rho_1 = \rho_2 = \rho_3 = 0$ of T_{ABC} can only exist in the region of parameters lying outside the three right-angled cones.

Therefore, the fixed points that differ only in the sign of the third equation in (2.12) will collide when $A^2 = C^2 + B^2$.

Notice that the existence region of the trivial fixed point ($\rho_i = 0$) in the parameter space (A, B, C) has a conical shape with its tip touching the origin of the A axis. We believe that the existence regions of higher order cycles have similar configurations. This is a three-dimensional analog of the Arnold tongues in circle maps[15] typically exemplified by

$$T_{K\Omega}(\theta) = \theta + \frac{K}{2\pi} \sin 2\pi\theta + \Omega$$

In T_{ABC}, the parameter A plays the role of the external frequency Ω. In the integrable limit of both cases a specific cycle exists only for a given value of the frequency parameter. When the nonlinearity is increased, the cycles exist in a finite interval of frequency values. Since in T_{ABC} there are two nonlinearity parameters rather than one, the generalized Arnold tongues are three-dimensional objects. Moreover, these are only existence tongues, while in $T_{K\Omega}$ they indicate the stability of cycles as well. Numerical investigations of the tongue structure for T_{ABC} are in progress and will be reported in a future publication.

2.3. Symmetries and Reversibility

A knowledge of the symmetries present in the mapping equations is useful for the understanding of many aspects of the dynamics. The sym-

metries are reflected, for instance, in the location of invariant objects in the phase space as well as in their properties. In particular, reversibility is a symmetry that has been proven to be crucial in allowing the extension of some results of the Hamiltonian theory to more general dynamical systems in even dimensions.[16] In general, a map T is called reversible with respect to an involutive transformation S (i.e., a transformation such that $S^2 = \text{identity}$) if $T^{-1} = S \circ T \circ S^{-1} = S \circ T \circ S$. As before, we will employ the ABC map to illustrate the nature of the symmetries. In the next subsection we will describe some remarkable implications of these symmetries for the stability of the trajectories.

In T_{ABC}, as opposed to the ABC flow, there are two different variables for each space direction: the variable before the propagation and the variable after (the primed variables). As a consequence, most symmetries of the ABC flow break down following the discretization. However, both the flow and the map are invariant under $\mathbf{r}_i \to \mathbf{r}_i + \pi$ and $\mathbf{Q}_i \to -\mathbf{Q}_i$, where $i = 1, 2, 3$, $\mathbf{r} = (x, y, z)$, and $\mathbf{Q} = (B, C, A)$. This enables us to limit our investigations to the positive octant, for which $A > 0$, $B > 0$, $C > 0$. Moreover, when $A = B$, $T_{AAC} \equiv T_{ABC}$ $(A = B)$ is invariant under S_P as well,

$$S_P: \quad (t, x, y, z) \to (-t, -z + \pi/2, -y + \pi/2, -x + \pi/2) \tag{2.14}$$

S_P is an involution $S_P^2 = I$ and therefore T_{AAC} is reversible.[16] The invariance under S_P implies

$$S_P \circ T_{AAC} \circ S_P^{-1} = T_{AAC}^{-1} \tag{2.15}$$

where $\circ$ denotes functional composition. In a more pictorial way, Eq. (2.15) reads

$$\begin{array}{ccc} P_0 & \xrightarrow{S_P} & P_1 \\ {\scriptstyle T_{AAC}}\downarrow & & \downarrow{\scriptstyle T_{AAC}^{-1}} \\ P_0' & \xrightarrow[S_P]{} & P_1' \end{array} \tag{2.16}$$

In Appendix A we prove an important property of reversible 3D maps. Namely, that whenever the Jacobian matrix of the involution ∂S is not dependent on the coordinates (as in S_P) the eigenvalues of the linearized map ∂T at the two points P_0 and $P_1' = S_P \circ T_{AAC}(P_0)$ are inverses of each other. Moreover, if P_0 is a fixed point $(P_0 = P_0')$, then also $P_1 = P_1'$ and therefore the same result is obtained without the requirement that ∂S is constant. In other words, in an arbitrary reversible map, each fixed point has a companion with inverse eigenvalues. When $A \neq B \neq C$ we are not

able to find explicitly an involution S_P as before and perturbative calculations suggest that it has a complicated form. However, an indication of its existence can be found in the fact that the fixed points are coupled in pairs with inverse eigenvalues, as is also shown in Appendix A. One striking implication of these results will be discussed in the next subsection.

2.3. In Reversible Maps the Second Liapunov Exponent Is Zero

We have anticipated that for large values of A, B, and C the map T_{ABC} displays only chaotic motion. A useful characterization for this kind of motion is given by the Liapunov exponents. In three dimensions, there are in general three independent exponents $\lambda_1 \geqslant \lambda_2 \geqslant \lambda_3$,[17]

$$\lambda_1 = \mu_1; \qquad \lambda_2 = \mu_2 - \lambda_1; \qquad \lambda_3 = \mu_3 - \lambda_2 - \lambda_1 \tag{2.17a}$$

$$\mu_i = \lim_{n \to \infty} \frac{1}{n} \log \frac{|\partial T^n(x_0)\, \mathbf{e}_1 \times \cdots \times \partial T^n(x_0)\, \mathbf{e}_i|}{|\mathbf{e}_1 \times \cdots \times \mathbf{e}_i|} \tag{2.17b}$$

for almost all choices of the three linearly independent vectors $\mathbf{e}_j$. In our example, however, the volume-preserving property implies $\lambda_1 + \lambda_2 + \lambda_3 = 0$. Consequently, there are only two relevant exponents. Roughly speaking, λ_i can be considered as the averaged logarithm of the Jacobian matrix eigenvalues over one trajectory of the map T. The numerical determination of the Liapunov exponents for the ABC map surprisingly shows that λ_2 vanishes for every examined combination of the parameters in the chaotic region. One possible explanation for this fact is based on the reversibility property. We have seen that if the involution is linear, this property implies that every point in the space will have a corresponding companion with inverse eigenvalues. For a trajectory that visits both points with equal probability, the contribution of each one to λ_2 will cancel the contribution of the other. Notice that for this type of trajectory the argument can be extended to the case where the involution is nonlinear if we assume that the fixed points and cycles are distributed with the same measure as the parts of the chaotic trajectory.

3. INVARIANT STRUCTURES AND DIFFUSION IN 3D MAPS

This section is devoted to one of the main questions regarding 3D maps: whether Arnold diffusion is present in the various nearly integrable cases. The actual existence of diffusion depends on the behavior of the invariant structures under nonlinear perturbations. In the 2D standard map, for example, this diffusion is forbidden because the invariant lines

that foliate the phase space in the integrable case survive to some extent when the nonlinearity is present. Any pair of those lines block the escape of the chaotic trajectories lying between them. A similar behavior should occur in the 3D case, provided that the appropriate invariant surfaces persist at finite nonlinearities.

We can further pursue the analogy between the 2D and 3D maps for the case with only one action. In the former, invariant lines with rational rotation numbers (resonant lines) break under perturbation into an even number of fixed points through a Poincaré–Birkoff mechanism. Half of the fixed points are elliptic and half are hyperbolic. Similarly, in the 3D case resonant invariant planes break into an even number of stable and unstable invariant curves. The elliptical islands enclosing the stable fixed points in the perturbed 2D map correspond to the elliptical invariant tubes surrounding stable lines of the 3D case. Around unstable fixed points (invariant curves) and their corresponding separatrices, strips (layers) of chaotic motion emerge. The chaotic regions are separated from each other and diffusion from one to another will be possible only after the last separating invariant curve (surface) breaks down. Earlier work on the standard map used sequences of fixed and cyclic points approximating the invariant curves to investigate the nature of the onset of diffusion. For 3D maps, we expect that an analogous role will be played by sequences of invariant or cyclic curves remaining after the destruction of resonant planes.

For two actions the situation is different. In three dimensions the maps have invariant lines as integrable structure, but these do not divide the space into disconnected parts. We therefore could imagine that even very small nonlinearities might generate a tenuous web of interconnected chaotic regions, allowing diffusion through all the space. Moreover, it is not clear *a priori* whether a theorem analogous to the KAM one might also hold for this type of integrable structure. To gain insight into this point, let us pursue the comparison with 2D maps. A "two-action" 2D map is a perturbation of the identity. The identity itself is the "integrable" map under which every point in the space is mapped onto itself. At zero perturbation each point is an invariant. But for small perturbations the map behaves exactly like a flow and all the invariant points will slowly drift along the trajectories of that flow. Thus, the invariant structures are not really points, but a family of curves. Since any two-dimensional flow is integrable, the disappearance of the fixed points does not imply any chaotic properties of the map. Similarly, for 3D two-action maps, the first effect of the perturbation is to break down the invariant lines and replace these by a set of surfaces. In other words, the slow drifting of action variables (invariant lines) combines with the fast perpendicular angular motion to

generate invariant surfaces. However, the fact that, according to Eq. (1.6), the fast motion becomes resonant on surfaces that are independent of the invariant ones has important implications in the 3D case. Namely, one then has two possibilities. For some maps and in some regions of the space, the invariant surfaces do not intersect the resonance sheets and therefore are true invariants, which really do divide the space. On the other hand, when such intersections do occur, resonances can locally "destroy" or rather interconnect all the surfaces in a given region. These connections allow for a random motion, which in principle can cover the whole space and is analogous to Arnold diffusion.

3.1. KAM-like Behavior of One-Action Maps: Numerical Evidence

In order to visualize trajectories of 3D maps, the so-called slice method is used. We select a thin planar slice from the (x, y, z) space and record only these iterations that lie in it. For the 2D presentation we project those points on a 2D plane parallel to the section. Therefore, even sections of regular trajectories lying on a 2D invariant surface could appear in the slice as fuzzy curves under sufficient magnification. However, the fuzziness is bound to decrease as we make the slice width smaller. Throughout this paper a slice width of $2\pi/100$ is used. Notice that each section contains only partial information about the phase portrait and therefore a set of slices is needed to visualize the actual nature of the trajectories.

We will continue the study of the one-action maps employing the T_{ABC} example. To start with, we plot in Fig. 2 two perpendicular slices of the trajectories of T_{ABC} close to the integrable case. Specifically, we set $A = 1.5$, $B = 0.08$, $C = 0.16$ and iterate $5 \cdot 10^4$ times each of the 20 initial conditions equally spaced along the axis of the action variable z. The picture is reminiscent of the phase portrait for the 2D standard map. For simplicity, let us confine our discussion to the (x, z) slice. First note the sections of the perturbed invariant surfaces, which appear as a family of slightly deformed lines. The integrable invariant planes neighboring $z = 0$ and $z = \pi$ suffer a rather drastic change under perturbation. Around $x = \pi/2$, $z = 0$ and $x = 3\pi/2$, $z = \pi$ we can see elliptical curves forming a structure similar to that around stable fixed points in 2D area-preserving maps. In the present case, however, those closed curves are sections of a family of "coaxial" invariant tubes that surround an invariant line. In the next subsection we show, using perturbation expansions, that these lines are the remnants of planes that satisfy the resonance condition. According to (2.9), we can classify these resonant lines by the triplet of integers (m, n, k). For the z

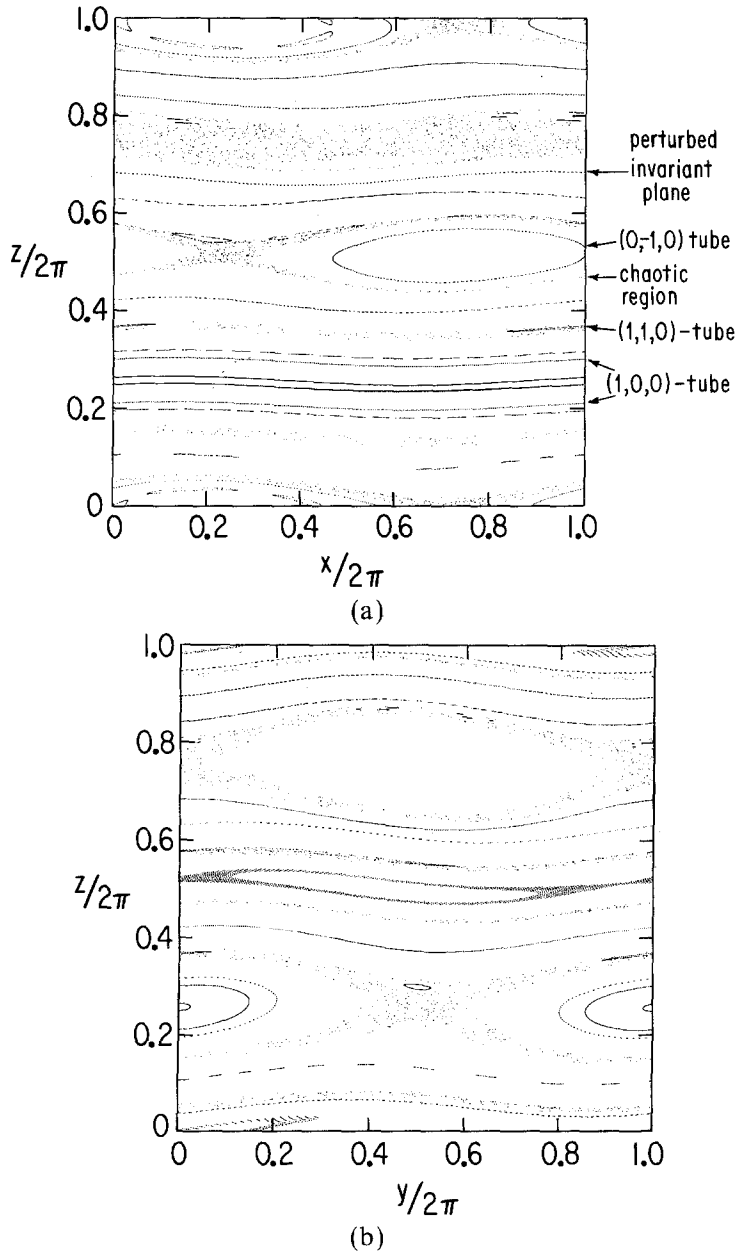

Fig. 2. Two perpendicular slices of 20 trajectories for T_{ABC} at $A = 1.5$, $B = 0.08$, and $C = 0.16$. The slices are in the (0, 0.01) interval of the perpendicular coordinate. Initial conditions are equally spaced along the z axis. Notice that this set of initial conditions generates three coaxial tubes around the (1, 0, 0) surviving invariant line.

values given before, $\rho_1 = 0$ and $\rho_2 = \pm A/2\pi$, and therefore the tubes correspond to the $(0, \pm 1, 0)$ resonant lines of the integrable map T_A. The curves between $z/2\pi \approx 0.19$ and $z/2\pi \approx 0.31$ are not sections of invariant planes as one might think, but longitudinal sections of a tube parallel to the x axis, as is confirmed by Fig. 2b. This tube corresponds to the $(1, 0, 0)$ resonance. A schematic 3D picture of all lowest order tubes is given in Fig. 3. Tubes emerging from higher order resonances are observed, for example, at $z/2\pi \approx 0.37$. This tube, which is more evident in Fig. 4, is a consequence of the $(1, 1, 0)$ resonance. This resonance corresponds to the case where the rotation numbers of the integrable trajectory satisfy $\rho_1 + \rho_2 = A \cos z_0 + A \sin z_0 = 0$.

In addition to the stable invariant lines, there are an equal number of unstable hyperbolic lines remaining from the destroyed resonant planes. The lowest order ones are located at $x = 3\pi/2$, $z = 0$; $x = \pi/2$, $z = \pi$; $y = \pi$, $z = \pi/2$; and $y = 0$, $z = 3\pi/2$. Even though they are not apparent in Fig. 2, their existence is manifested in the form of chaotic trajectories. These trajectories fill layers that surround the tubes and are bounded by the deformed invariant planes. As the small parameters are increased, the chaotic regions grow in size at the expense of invariant surfaces. Figure 4 is analogous to Fig. 2, but for $A = 1.5$, $B = 0.1$, and $C = 0.2$. Regular and chaotic trajectories still coexist, but the latter are dominant.

In Fig. 2 we clearly see the invariant surfaces separating all chaotic regions from each other. It is shown in Appendix B that the existence of those surfaces prevents diffusion from one chaotic region to another. Some

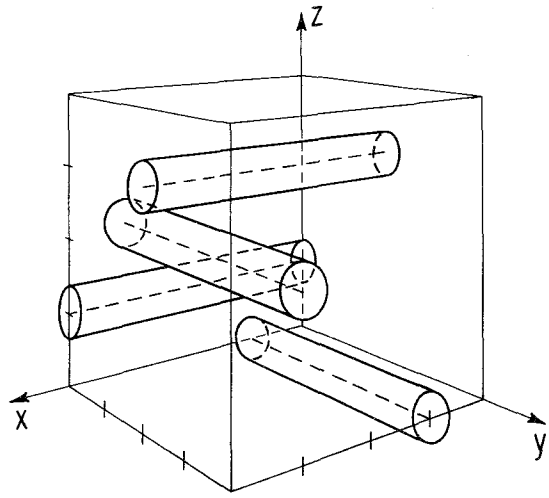

Fig. 3. A three-dimensional schematic representation of the four $A < 2\pi$ tubes of T_{ABC}.

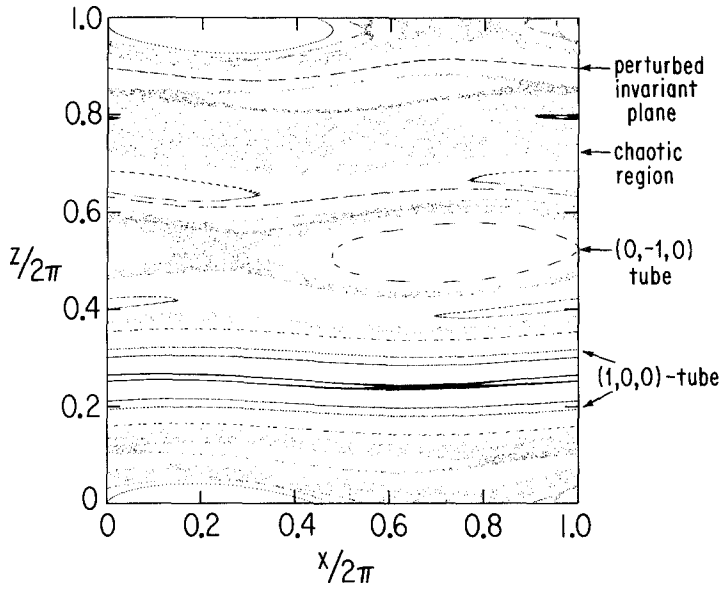

(a)

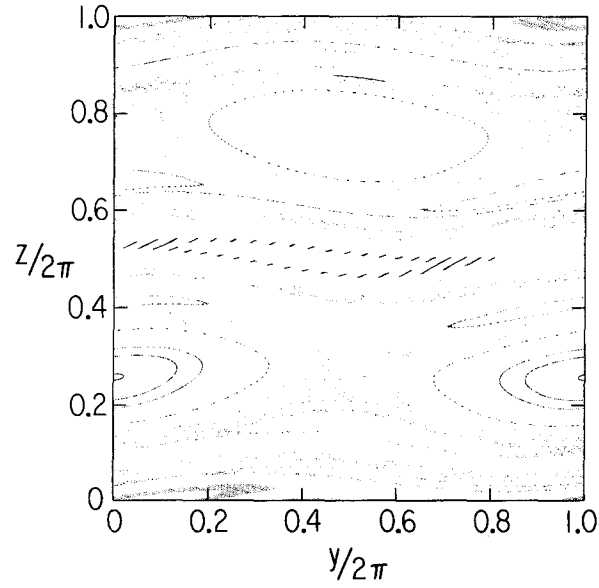

(b)

Fig. 4. Two slices of 20 trajectories of T_{ABC} as in Fig. 2, only here $A = 1.5$, $B = 0.1$, and $C = 0.2$.

of the surfaces are also present in the case depicted in Fig. 4. They would be in the blank areas around $z/2\pi \approx 0.08$ and $z/2\pi \approx 0.85$, but our grid of initial conditions is not dense enough to resolve them. One perturbed invariant plane is displayed Fig. 5 by simply projecting the trajectory down on one plane instead of using the slice method. The fact that these perturbed invariant planes really block diffusion for finite values of B and C can also be numerically checked. For $C = 2B$ we measure the time $t_E(B)$ it takes a chaotic trajectory starting from the $z = 0$ plane to reach the one at $z = 2\pi$. Starting from high values of B for $A = 1.5$, t_E is found to diverge at finite B. A good fit to T_E is found in the form

$$t_E(B) = \frac{t_0}{(-B/B_0 + 1)^{\alpha}} \tag{3.1}$$

and gives $t_0 \approx 3$, $B_0 \approx 0.117$, and $\alpha \approx 2.2$. This indicates the absence of Arnold diffusion for T_{ABC}. Moreover, in the following subsection, we show that the perturbation expansions for 3D one-action maps lead to the same small-denominator problems as in, for example, the two-dimensional standard maps. Apparently a kind of KAM mechanism also holds in 3D maps with only one action.

3.2. Perturbation Expansions for One-Action Maps

As before, we use the ABC map as a representative of one-action maps.

3.2.1. Invariant Surfaces. We have shown in Section 2.2 that when $B = C = 0$, the space is foliated by the planes $z = z_0 = \text{const}$, which are invariant under T_A. Since we are interested in the persistence of this invariant structure for small but finite values of B and C, we will implement a perturbative scheme to obtain the invariant surfaces corresponding to each plane. Let us take $B = \alpha_B \varepsilon$ and $C = \varepsilon$ with ε small. We therefore assume that the surfaces can be represented by the equation

$$z = z_0 + \sum_{n=1}^{\infty} \varepsilon^n H_n(x, y) \tag{3.2}$$

The second ingredient of the scheme is the requirement given by Eq. (2.5) that a point on an invariant surface has to remain on it under the iteration of the map. Substituting (3.2) into (2.5) with the obvious identification $(t, s) \to (x, y)$, we obtain in general an infinite set of linear functional equations for the H_n. These equations can in principle be solved order by

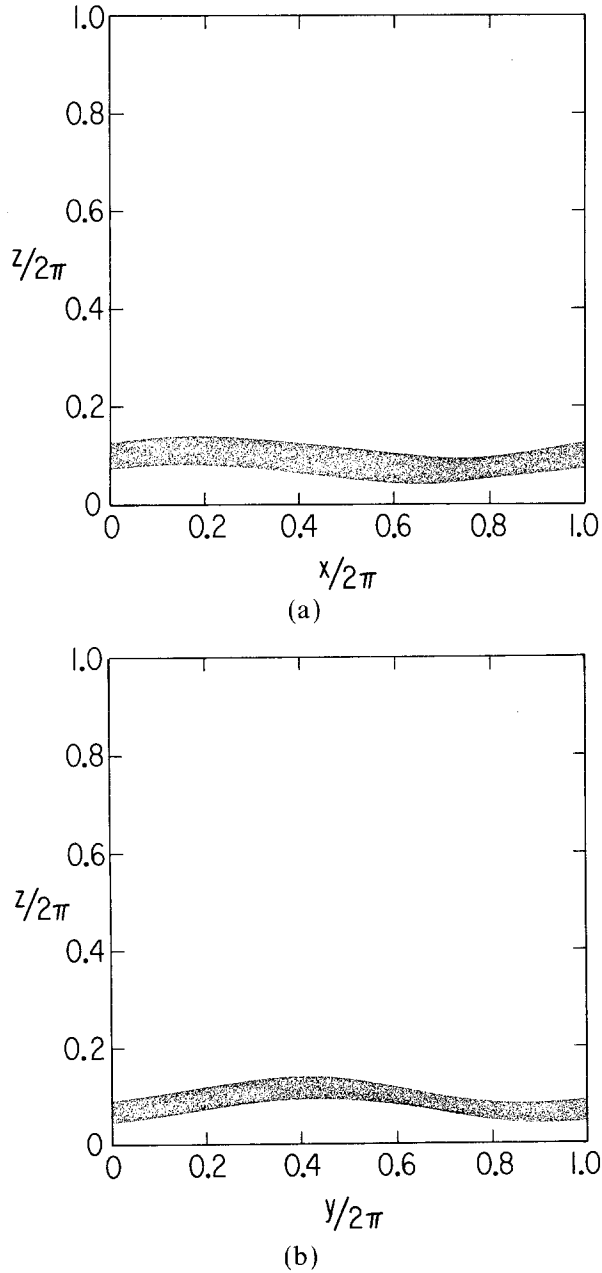

Fig. 5. Three perpendicular projections of an invariant plane for T_{ABC} at $A = 1.5$, $B = 0.1$, and $C = 0.2$.

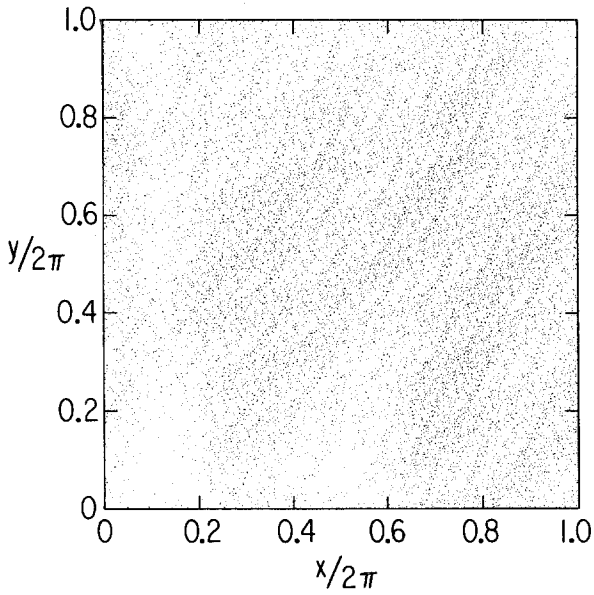

(c)

Fig. 5 (*continued*)

order. Let us restrict ourselves to first-order calculations for the invariant surfaces. Equations (2.3), (2.5), and (3.2) lead us to

$$\begin{aligned} x' &= x + A \sin z_0 + \varepsilon \cos y \\ y' &= y + A \cos z_0 + \varepsilon \alpha_B \sin x' \\ z' &= z_0 + \varepsilon H_1(x', y') + O(\varepsilon^2) \\ &= z_0 + \varepsilon H_1(x + A \sin z_0,\ y + A \cos z_0) + O(\varepsilon^2) \\ &= z_0 + \varepsilon H_1(x, y) + \varepsilon \sin(y + A \cos z_0) + \varepsilon \alpha_B \cos(x + A \sin z_0) + O(\varepsilon^2) \end{aligned} \tag{3.3}$$

$H_1(x, y)$ therefore satisfies the linear functional equation

$$\begin{aligned} &H_1(x + A \sin z_0,\ y + A \cos z_0) \\ &\quad = H_1(x, y) + \sin(y + A \cos z_0) + \alpha_B \cos(x + A \sin z_0) \end{aligned} \tag{3.4}$$

which can be easily solved by expanding $H_1(x, y)$ in a double Fourier series. Since H_1 has to be periodic, we have in general

$$H_1(x, y) = \sum_{m,n=-\infty}^{\infty} a_{mn} e^{i(mx+ny)} \tag{3.5}$$

From (3.4) and (3.5) we obtain the equation for a_{mn},

$$a_{mn}\{\exp[i(mA\sin z_0 + nA\cos z_0)] - 1\}$$
$$= \tfrac{1}{2}i[\delta_{-1,n}\exp(-iA\cos z_0) - \delta_{1,n}\exp(iA\cos z_0)]\,\delta_{0,m}$$
$$+ \tfrac{1}{2}\alpha_B[\delta_{1,m}\exp(iA\sin z_0) + \delta_{-1,m}\exp(-iA\sin z_0)]\,\delta_{0,n} \quad (3.6)$$

A solution can be obtained with the only nonzero terms being $a_{0,\pm 1}$ and $a_{\pm 1,0}$. The resonance condition

$$mA\sin z_0 + nA\cos z_0 = 2\pi k \quad (3.7)$$

gives no trouble at this order as long as (m, n, k) is not equal to $(\pm 1, 0, k)$ or $(0, \pm 1, k)$. Thus, T_{ABC} displays what we call a separation of orders: $H_r(x, y)$ contains only the Fourier coefficients a_{mn} for which $|m| + |n| = r$. Therefore, each order-in-ε correction to the invariant surface generates only a_{mn} of given order, leaving unchanged the Fourier coefficients of different r. The $a_{0,\pm 1}$ and $a_{\pm 1,0}$ expressions in Eq. (3.6) are correct to all orders in ε.

3.2.2. Tubes. The condition (3.7) has a special set of consequences when it holds for $(m, n, k) = (\pm 1, 0, k)$ and $(m, n, k) = (0, \pm 1, k)$. In this cases the values of $a_{0,\pm 1}$ and $a_{\pm 1,0}$, respectively, diverge, the expansion breaks down, and, in fact, the invariant surface disappears. For those values of (m, n, k), Eq. (3.7) is equivalent to

$$A\sin z_0 = 2\pi k_1; \qquad A\cos z_0 = 2\pi k_2 \quad (3.8)$$

When $A < 2\pi$ there are resonances only for $k_1 = k_2 = 0$. These are located at $z_0 = 0, \pi$ and $z_0 = \pi/2, 3\pi/2$ and correspond to the $(0, \pm 1, 0)$ and $(\pm 1, 0, 0)$ resonant lines of T_A (see Section 2.2), respectively. Around these resonances, invariant planes break down and form tubular structures, as described in Section 3.1. The tubes arising from the singularity in $a_{\pm 1,0}$ are parallel to the y direction, while the $a_{0,\pm 1}$ ones are in the x direction.

When $A = 2\pi$, eight new tubes are generated in addition to the $A < 2\pi$ four. These are $k_1 = k_2 = 1$ solutions to Eq. (3.8) and are located at the middle points (in z) between the $k_1 = k_2 = 0$ tubes. At each middle point there are two new y tubes (x tubes): one at $x = \pi/2$ ($y = \pi/2$) and the other at $x = 3\pi/2$ ($y = 3\pi/2$). Each emerging tube migrates away from its creation position as A grows, one toward lower z and the other to higher z. Every time A passes through a multiple of 2π (say $A = 2\pi l$, with l being an integer), a new generation of eight tubes appears, as in the $l = 1$ case. If we consider only the tubes parallel to the y direction, we now have $4l$ of the type that change position with A and two fixed ones. The migrating tubes accumulate as $l \to \infty$ at both sides of the two fixed ones. This

accumulation-like picture is further emphasized by the fact that the migrating tubes are around the same x value as the fixed tube they are moving toward.

Let us concentrate for a while on the appearance of the $l=1$ tubes. It turns out that the structure described in the previous paragraph is further enriched by the interaction among x and y tubes. Since at the z value where the new x tubes are generated the original y tubes are also located, this interaction is especially strong at $A=2\pi$. The new x tubes and the old y tubes have a spatial oscillation modulated such as to avoid each other. But this avoidance is not always strong enough. The tubes degenerate into chaotic motion whenever they come too close to one another. To illustrate this phenomenon, we look at a case in which B and C are quite small, $B=0.01$ and $C=0.02$. In Fig. 6, $A=6.3$, so we are just above the point where the first set of migrating tubes should have appeared. One can see that at this A value all fixed tubes become chaotic due to collisions with the emerging new ones. However, as A is further increased and the new tubes migrate away, all tubes reappear and the amount of chaotic motion in their region dwindles (see Fig. 7). The relative amount of chaotic motion in the tube region is maximal at $A=2\pi$ and decays as A is either increased or decreased from this critical value.

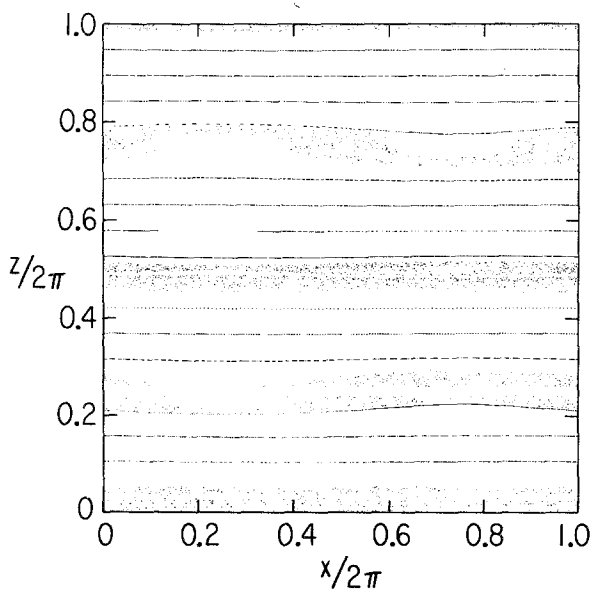

Fig. 6. The (x, z) slice for T_{ABC}. Parameters are $A=6.3$, $B=0.01$, and $C=0.02$. Collisions of old and new tubes generate layers of chaotic motion where the tubes should be.

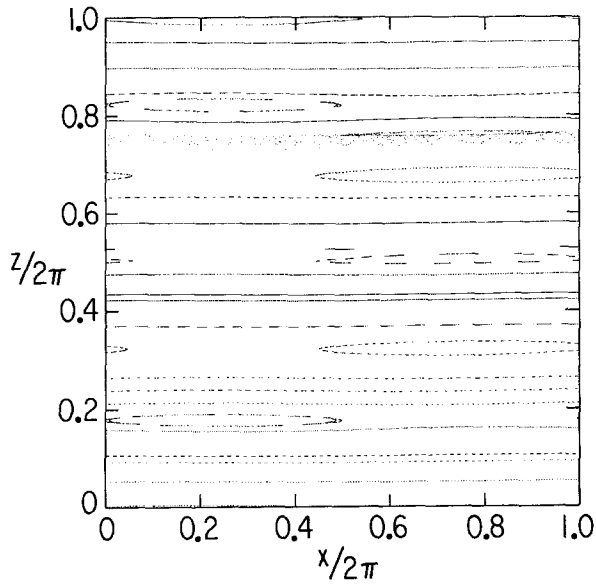

Fig. 7. Same as in Fig. 6, only here $A = 7$. Both new and old tubes have reappeared in the positions predicted by Eq. (3.8).

Far from the singularities of the Fourier coefficients in Eq. (3.5), the constant z invariant planes of the integrable case evolve into slightly undulated ones (see Fig. 5). Up to first order in ε, the expression for the perturbed invariant planes is derived from Eqs. (3.2), (3.5), and (3.6). We obtain

$$z = z_0 + \frac{\varepsilon}{2}\frac{\sin y - \sin(y + A\cos z_0)}{1 - \cos(A\cos z_0)} + \frac{\varepsilon\alpha_B}{2}\frac{\cos x - \cos(x + A\sin z_0)}{1 - \cos(A\sin z_0)} \tag{3.9}$$

Equation (3.9) can be used to evaluate the location of the tube separatrices and therefore the size of the resonant regions. This will allow us to estimate the parameter values for which chaos sets in via the Chirikov resonance overlap criterion. A calculation in this spirit is presented in Appendix C. We obtain that, for $A < 2\pi$, whenever

$$\frac{3}{2}\left(\frac{2B}{A}\right)^{1/2} \geqslant \frac{\pi}{4} \tag{3.10}$$

motion becomes chaotic through the overlap of the $(0, 1, 0)$ and the $(0, -1, 0)$ resonances. For example, at $A = 1.5$, Eq. (3.9) gives $B \approx 0.2$ for the onset of chaos. Thus, the resonance criterion overestimates by a factor of about two the value $B \approx 0.117$ for the onset which was obtained

numerically in Eq. (3.1). This situation is reminiscent of the one observed in the standard map (see Ref. 9, p. 227).

3.2.3. Invariant Lines. The preceding discussion concerning the tubular structures arising from the resonant planes was mainly qualitative. Building a more precise description of these structures is a difficult task. In 2D maps the analysis of the corresponding objects proceeds easily by linearizing the map around the elliptic fixed points which appear according to the Poincaré–Birkoff mechanism. Those points are solutions of algebraic equations and their stability is a 2×2 eigenvalue problem. For 3D maps instead the invariant lines remaining from the destroyed resonant planes are solutions of a nonlinear functional equation and their stability analysis leads to an infinite eigenvalue problem. Even the numerical determination of those lines is a hard problem. In the following we will employ perturbation theory to give an approximate expression for those lines in the one-action case. Let us consider the first-order resonant planes $(0, \pm 1, 0)$ at $z = 0, \pi$. We have shown in Section 2.2 that at $\varepsilon = 0$ the iterations of T_{ABC} lie on lines parallel to the y axis. Each initial condition x_0 corresponds to a different line, which is then defined by $x = x_0$ and $z = z_i$, where $z_1 = 0$ and $z_2 = \pi$. We want to understand what happens to these lines when $\varepsilon \neq 0$. Therefore, we look for perturbed lines of the form

$$x = x_0 + \varepsilon X(y) + O(\varepsilon^2); \qquad z = z_i + \varepsilon Z(y) + O(\varepsilon^2) \tag{3.11}$$

and confine our calculations to order ε. Using the invariance condition (2.4), we now obtain two functional equations, one for $X(y)$ and another for $Z(y)$,

$$X[y + A\cos z_i] = X(y) + AZ(y)\cos z_i + \cos y \tag{3.12a}$$

$$Z[y + A\cos z_i] = Z(y) + \sin(y + A\cos z_i) + \alpha_B \cos x_0 \tag{3.12b}$$

Using the periodicity of the boundary conditions, we expand both $X(y)$ and $Z(y)$ in Fourier series

$$X(y) = \sum_{n=-\infty}^{\infty} a_n^x e^{iny}; \qquad Z(y) = \sum_{n=-\infty}^{\infty} a_n^z e^{iny} \tag{3.13}$$

The Fourier coefficients satisfy

$$a_n^x[\exp(inA\cos z_i) - 1] = A(\cos z_i)\, a_n^z + \tfrac{1}{2}(\delta_{1,n} + \delta_{-1,n}) \tag{3.14a}$$

$$a_n^z[\exp(inA\cos z_i) - 1] = \tfrac{1}{2}i[\delta_{-1,n}\exp(-iA\cos z_i) - \delta_{1,n}\exp(iA\cos z_i)] + \delta_{0,n}\alpha_B \cos x_0 \tag{3.14b}$$

Now we can show how the perturbation expansion allows one to visualize the Poincaré–Birkoff-like mechanism by which resonant planes break into a finite set of invariant lines. Equation (3.14b) displays a spectacular type of singularity, which results from the nonvanishing term of Fourier order zero. For $n=0$ the factor $[\exp(inA\cos z_i)-1]$ vanishes and therefore Eq. (3.14b) cannot be satisfied unless $\cos x_0 = 0$. Only four $(0, \pm 1, 0)$ lines of T_A satisfy this condition; the (x_0, z_i) pairs that define these are $(\pi/2, \pi)$, $(3\pi/2, 0)$, $(\pi/2, 0)$, $(3\pi/2, \pi)$. In other words, out of the infinite set of lines of the integrable case, only four survived the presence of the nonlinear perturbation. This is analogous to the way in which resonant invariant curves of 2D maps break under nonlinear perturbation into pairs of fixed points. The $(\pi/2, 0)$, $(3\pi/2, \pi)$ surviving invariant lines are axes of the two families of elliptical tubes observed in Figs. 2a and 4a. This indicates that they are stable. Each of the other two, instead, is located at the core of a corresponding hyperbolically shaped chaotic layer, which suggests that they are unstable.

Since the coefficients of a_n^x and a_n^z in Eqs. (3.14a) and (3.14b) vanish at $A = 2\pi l$, even the two stable surviving lines are bound to break close to the critical A values. This provides an alternative explanation for the enhancement of chaos at $A = 2\pi$ in the tube region.

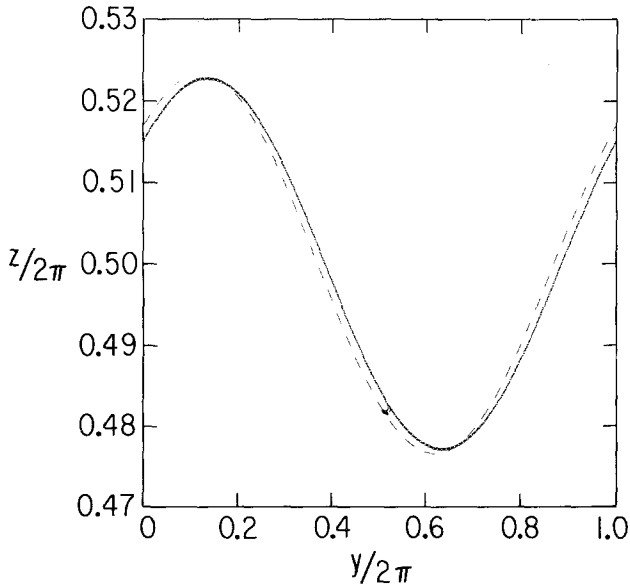

Fig. 8. Comparison of $z(y) = z_2 + \varepsilon Z(y)$, where $Z(y)$ is given by Eq. (3.15b) (dashed line), with the (y, z) projection of the central line in the $(x = 3\pi/2,\ z = \pi/2)$ y-tube. Parameters of T_{ABC} are the same as in Fig. 5.

If nonsingular, the solutions to Eq. (3.13) can be obtained after some algebra. For the lines with $z = z_2 = \pi$

$$X(y) = -\frac{A}{2}\frac{\sin(y+A) - 2\sin y + \sin(y-A)}{3 - 4\cos A + 2\cos 2A} + \frac{\cos(y+A) - \cos y}{2(1-\cos A)} \tag{3.15a}$$

$$Z(y) = \frac{\sin y - \sin(y-A)}{2(1-\cos A)} \tag{3.15b}$$

The same expression with $A \to -A$ give the solutions for the $z = z_1 = 0$ invariant lines. In Fig. 8 we compare the perturbative invariant line given by Eqs. (3.11) and (3.15b) with the numerically obtained one at the center of the y tube at $(x = 3\pi/2,\ z = \pi)$. The disagreement between the two is consistent with our expected error, which is of order ε^2.

3.3. Perturbation Theory for Two-Action Maps: Diffusion

In this section we study the class of maps T_{II} defined by setting $A_1 = \varepsilon$, $A_2 = \alpha_{A2}\varepsilon$, $B_1 = \alpha_{B1}\varepsilon$, and $C_2 = \alpha_{C2}\varepsilon$ with $\varepsilon \ll 1$ in Eq. (2.3) and leaving the remaining parameters and the functions of order unity,

$$\begin{aligned} x' &= x + \varepsilon\alpha_{A1}\sin z + \varepsilon\alpha_{C2}\cos y \\ y' &= y + \varepsilon\alpha_{B1}\sin x' + \varepsilon\alpha_{A2}\cos z \\ z' &= z + C_1 f(y') + B_2 g(x') \end{aligned} \tag{3.16}$$

Under these conditions x and y (actions) are nearly conserved under iteration, while z (angle) varies rapidly. When $\varepsilon = 0$ the conservation of the actions is exact and all the trajectories lie on lines defined by $x = x_0$, $y = y_0$. Notice that these lines fill the whole space, while in the previously studied one-action case, the invariant lines are of zero measure. In order to investigate the behavior at $\varepsilon \neq 0$ we will use the same procedure as in (3.2). Since the lines are parallel to the z axis, we suppose that the perturbed ones are given by

$$x = x_0 + \varepsilon X(z) + O(\varepsilon^2); \qquad y = y_0 + \varepsilon Y(z) + O(\varepsilon^2) \tag{3.17}$$

Disregarding $O(\varepsilon^2)$ terms, we obtain the two functional equations for $X(z)$ and $Y(z)$:

$$X[z + C_1 f(y_0) + B_2 g(x_0)] = X(z) + \alpha_{A1}\sin z + \alpha_{C2}\cos y_0 \tag{3.18a}$$

$$Y[z + C_1 f(y_0) + B_2 g(x_0)] = Y(z) + \alpha_{B1}\sin x_0 + \alpha_{A2}\cos z \tag{3.18b}$$

Solving as usual by Fourier expansion, we find

$$a_n^x(\exp\{in[C_1 f(y_0) + B_2 g(x_0)]\} - 1)$$
$$= \frac{\alpha_{A1}}{2i}(\delta_{n,1} - \delta_{n,-1}) + \alpha_{C2}\delta_{n,0}\cos y_0 \tag{3.19a}$$

$$a_n^y(\exp\{in[C_1 f(y_0) + B_2 g(x_0)]\} - 1)$$
$$= \frac{\alpha_{A2}}{2}(\delta_{n,1} + \delta_{n,-1}) + \alpha_{B1}\delta_{n,0}\sin x_0 \tag{3.19b}$$

Note that a_0^x and a_0^y are both divergent unless the condition

$$\sin x_0 = \cos y_0 = 0 \tag{3.20}$$

is satisfied. According to Eq. (3.20), only the lines defined by the (x_0, y_0) pairs $(0, \pi/2)$, $(\pi, 3\pi/2)$, $(0, 3\pi/2)$, and $(\pi, 3\pi/2)$ will survive perturbation. The general breakdown of the invariant lines at order ε might lead one to expect that the whole invariant structure should disappear at arbitrarily small values of ε in favor of a completely diffusive motion. However, the invariant surfaces shown in Fig. 9 deny this expectation. There, the (x, y) slice of the trajectories of the map T_{IIa} obtained from Eq. (2.3) by setting

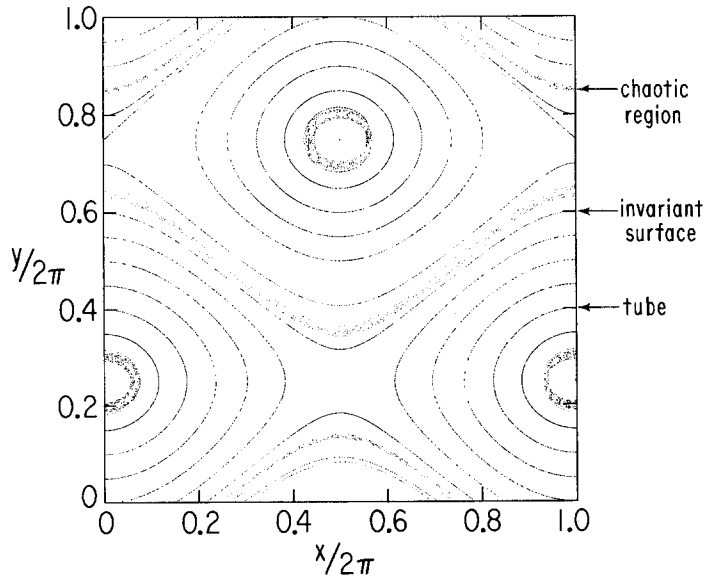

Fig. 9. The (x, y) slice of T_{IIa} with $A_1 = 0.001$, $B_1 = 0.0015$, $C_2 = 0.002$, $A_2 = 0.0025$, $C_1 = 2.5$, and $B_2 = 4$.

$f(y)=\sin y$ and $g(x)=\cos x$ is shown. A surprising new structure is displayed. Two of the four nonsingular lines are surrounded by a family of invariant tubes. Moreover, undulated invariant surfaces topologically equivalent to planes also appear. The separatrices between those surfaces and the tubes intersect at the other two "hyperbolic" lines. We conclude that under perturbations invariant lines coalesce, forming invariant surfaces. In other words, the integrable case consisting of a two-parameter family of invariant lines is actually a degenerate limit of another integrable case composed of a one-parameter family of invariant surfaces. We will show, however, that some of those surfaces break at order ε because of singularities due to the $\delta_{\pm 1,n}$ terms occurring when the $n=1$ resonance condition in

$$n[C_1 f(y_0)+B_2 g(x_0)]=2\pi k \tag{3.21}$$

is satisfied. The projection of the $(n,k)=(1,0)$ resonance sheet given by Eq. (3.21) is shown in Fig. 10 for the same T_{IIa} map. It coincides with the thin chaotic region between the invariant planes. The chaotic rings arising around the invariant lines correspond to the $(n,k)=(1,\pm 1)$ resonances not shown in Fig. 10.

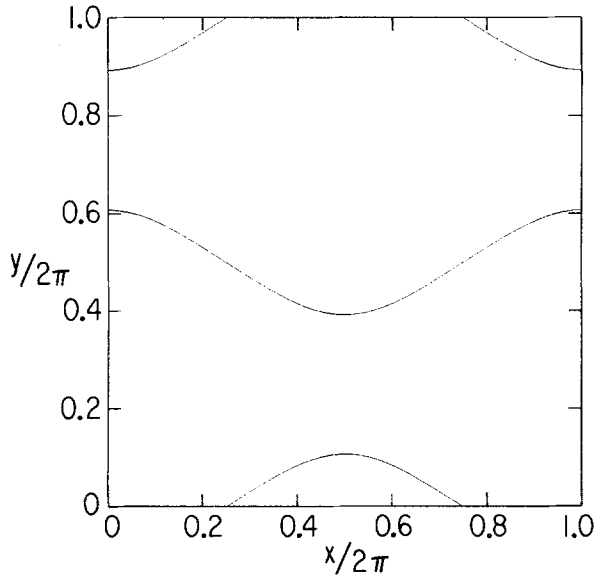

Fig. 10. Solutions of Eq. (3.21) with $(n,k)=(1,0)$. The C_1 and B_2 are the same as in Fig. 9 and therefore these are the lines on which the invariant curves W_β [see Eq. (3.23)] are resonant.

Let us show the origin of the above-mentioned invariant surfaces and the way they break if (3.21) is satisfied. First of all, when ε is extremely small (but nonzero) in T_{II}, z is a fast-moving variable, while x and y are very slow. Therefore, in the adiabatic limit we can separate the fast time scale by averaging over z and suppose that the (x, y) map is sensitive only to the averaged z terms. Assuming that z is uniformly distributed along $[0, 2\pi]$, the terms in T_{II} containing z average to zero. As a result, the slow map is

$$x' - x = \Delta x/\Delta n = \varepsilon\alpha_{C2} \cos y \tag{3.22a}$$

$$y' - y = \Delta y/\Delta n = \varepsilon\alpha_{B1} \sin x \tag{3.22b}$$

which closely resembles a flow. If we set $t = \varepsilon\, \Delta n$ and take the limit $\varepsilon \to 0$, the map of Eqs. (3.22a), (3.22b) actually becomes a flow. The trajectories of the resulting flow lie on curves W_β, which satisfy

$$B_1 \cos x + C_2 \sin y = \beta = \text{const} \tag{3.23}$$

Since there is an additional fast z motion whose frequency is typically incommensurate with that of the (x, y) motion, Eq. (3.23) describes the $\varepsilon \to 0$ invariant surfaces, which are the true integrable objects of T_{II}. Several W_β curves are shown in Fig. 11. Note the coincidence of these

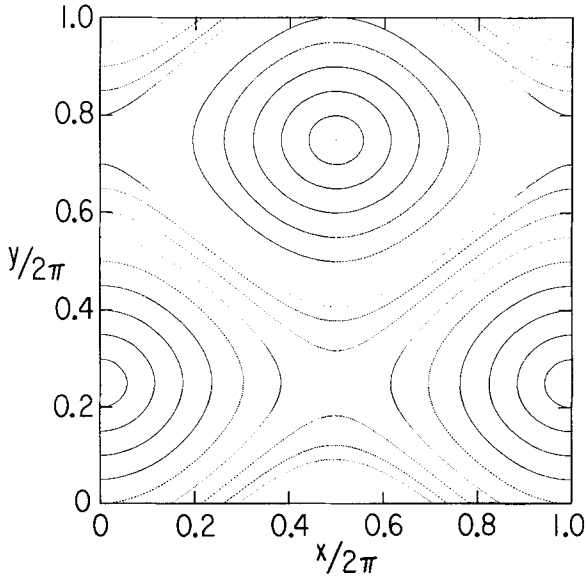

Fig. 11. The W_β curves of Eq. (3.23) with the same values for B_1 and C_2 as in Fig. 9. Moreover, the different curves have the same initial conditions as the trajectories shown in Fig. 9.

contours with the surfaces of Fig. 9. Notice also that the W_β curves do not depend on the choice of the f and g functions in T_{II}.

A meaningful perturbation theory can only be written for the surfaces of Eq. (3.23), but not for the invariant lines of the $\varepsilon = 0$ case. Let us pursue this line of thought. Up to order ε, the invariance condition for the perturbed W_β surfaces is

$$\begin{aligned} &B_1 \cos x' + C_2 \sin y' + \varepsilon H(x', y', z') \\ &\quad = B_1 \cos x + C_2 \sin y + \varepsilon H(x, y, z) \end{aligned} \tag{3.24}$$

From Eqs. (3.16) and (3.24) we can derive a functional equation for $H(x, y, z)$,

$$\begin{aligned} &H[x, y, z + C_1 f(y) + B_2 g(x)] - H(x, y, z) \\ &\quad = \alpha_{A1}\alpha_{B1} \sin x \sin z - \alpha_{A2}\alpha_{C2} \cos y \cos z \end{aligned} \tag{3.25}$$

Expanding $H(x, y, z)$ in a Fourier series in z,

$$H(x, y, z) = \sum_{n=-\infty}^{\infty} a_n(x, y)\, e^{inz} \tag{3.26}$$

we obtain the coefficients $a_n(x, y)$

$$\begin{aligned} &a_n(x, y)(\exp\{in[C_1 f(y) + B_2 g(x)]\} - 1) \\ &\quad = \delta_{1,n}\left(\frac{-i\alpha_{A1}\alpha_{B1} \sin x - \alpha_{A2}\alpha_{C2} \cos y}{2}\right) \\ &\qquad + \delta_{-1,n}\left(\frac{i\alpha_{A1}\alpha_{B1} \sin x - \alpha_{A2}\alpha_{C2} \cos y}{2}\right) \end{aligned} \tag{3.27}$$

We obtain the same singularity structure as in Eq. (3.21) and therefore a consistent explanation for the central band of chaotic trajectories in Fig. 9. The meaning of Eq. (3.27) is that the surfaces are (order ε) preserved under small perturbations, except at the intersection with the surface defined by the resonant condition (3.21). At the intersections, however, a local breakdown occurs. Consequently, the motion will follow the W_β surfaces as long as it is far from the resonance sheets. At the resonance the "pseudo-regular" trajectory $\tilde{W}_\beta$ is scattered off to a different one $\tilde{W}_{\beta'}$. Roughly speaking, the scattering processes induce a random walk among all W_β that intersect the surface of the singularities. We call this phenomenon singularity-induced diffusion (SID). We stress that in the case of T_{IIa} we have chosen the functions f and g such that the resonant sheets defined by (3.21) are almost coincident with the family of invariant surfaces W_β. Thus, only few W_β surfaces are crossed by the first-order ($n = 1$) resonances. Another extreme choice would allow almost all the surfaces to intersect

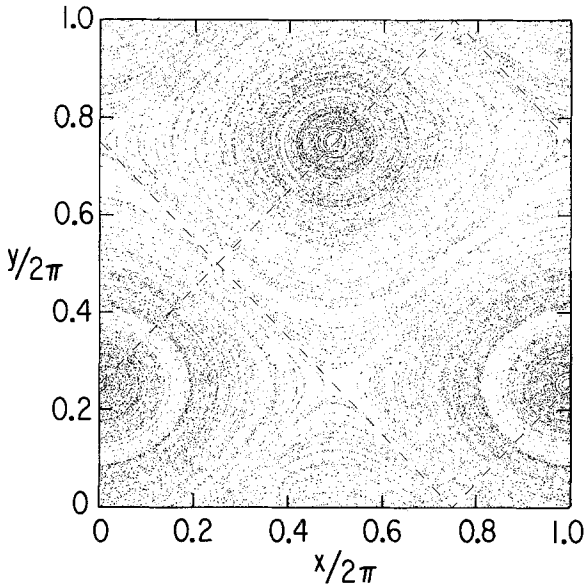

Fig. 12. The (x, y) slice of *one* trajectory for T_{IIb}. The small parameters are the same as in Fig. 9, while $C_1 = B_2 = 4$. The dashed lines indicate the position of the $(n, k) = (1, 0)$ singularities of Eq. (3.21).

with the first-order resonance sheet. Such an extreme is the map T_{IIb} defined by setting $f(y) = \cos y$, $g(x) = \sin x$, and $B_2 = C_1$. In Fig. 12 only one trajectory of T_{IIb} is shown to cover the whole space. Notice that here $\varepsilon = 10^{-3}$, which is two orders of magnitude less than in the case of the partially chaotic ABC map, as shown, for example, in Fig. 4. In intermediate cases the $n = 1$ resonance sheets do not intersect the whole W_β family, but only a compact fraction of it. However, since in the generic case higher order resonances are dense in the space, all the W_β surfaces intersect at least one of the sheets. The effect of these higher order resonances is similar to that of the first-order ones, but it is manifested on longer time scales. Therefore, except for nongeneric maps, SID is able to reach any region of the space. While the mechanism is different, the effects of SID are similar to those produced by Arnold diffusion. The nature of the local breakdown of the adiabatic invariants will be analyzed in detail elsewhere.

4. SUMMARY AND CONCLUSIONS

Due to the absence of canonical structure it is not trivial to extend the general results of the theory of Hamiltonian systems to 3D volume-preserving maps. However, combining the first steps of perturbation theory

with numerical evidence, we are in position to conjecture how this extension could work. First, a classification of the variables as action-like or angle-like according to their variability (slow for the former and fast for the later) proved to be useful for the understanding of the invariant structures close to integrability. The character of a given variable depends on the choice of the parameters. Disregarding the case of three actions, which is close to an autonomous 3D flow, and the case of three angles, which is generically chaotic, we are left with two types of maps: those containing one or two actions, respectively. For the former, we found that the action labels a one-parameter family of invariant surfaces (2-tori). Perturbative expansions and numerical evidence allow us to conjecture that a version of the KAM theorem holds in this case. For the second type, the integrable case is composed of a two-parameter (the two actions) family of invariant lines. The motion on those lines has a frequency that is degenerate along curves in the action plane. This degeneracy spoils the validity of the hypothesis of the KAM theorem and we do not expect a trivial extension of it to this case. However, we found that the adiabatic approximation provides us with a mechanism by which the broken lines regroup in invariant surfaces. The striking result is that those invariant surfaces survive when the coupling to the fast motion is increased. However, a cut in the surface appears due to the resonances of the fast motion. These resonances connect different invariant surfaces, giving rise to a new kind of Arnold diffusion, which we call singularity-induced diffusion. This diffusion is present no matter how small are the nonlinearities.

These results have important consequences for the mixing of passive scalars. Whenever the fast motion is restricted to surfaces, low mixing efficiencies are expected due to the existence of KAM barriers. On the contrary, if this fast motion is confined to just one direction, passive scalars will be typically scattered by resonances and an enhancement of diffusion in some regions of the space will be present.

We now propose an experimental realization for the enhanced transport phenomenon. Consider the two-vortex system proposed by Aref, but operating continuously. In the two-dimensional approximation this system is integrable and consequently a nonefficient stirrer. If instead of the blinking procedure we introduce a fast oscillatory flow in the third direction, the resonances associated with this motion will produce a diffusion of the particles, which could be controlled by adjusting the speed of the constantly (and slowly) moving agitators. Notice that in this *design* the tubes observed in Fig. 9 are equivalent to the vortices generated by the stirrers.

We cannot ensure that the tubes we found in many stages of our investigation are similar to visualization fluid vortices. Assuming, however,

that both objects are of the same type, some features found in our models, such as the appearance of new tubes as A is increased through multiples of 2π in T_{ABC}, could be observed experimentally.

Finally, we stress that due to the high codimension of this problem, the classification given above could be incomplete. Probably many new and interesting phenomena can be found in the extremely rich behavior of this kind of system.

APPENDIX A

In the first part of this appendix we prove that for maps T that are reversible with respect to the involution S, the eigenvalues of Jacobians at P_0 and $P_1' = S \circ T(P_0)$ are inverses of each other. We use the same notation as in Eqs. (2.15) and (2.16). Also, $T^S \equiv S \circ T \circ S^{-1}$ and therefore $T^S(P_1) = P_1'$. The linearized maps give

$$\partial T|_{P_0} \mathbf{r} = \lambda \mathbf{r}; \qquad \partial T^S|_{P_1} \mathbf{r}_S = \lambda_S \mathbf{r}_S \tag{A1}$$

where $\partial T|_P$ denotes the Jacobian of T at P. Then

$$\partial S|_{P_0'} \partial T|_{P_0} \partial S^{-1}|_{P_1} \cdot \mathbf{r}_S = \lambda_S \mathbf{r}_S \tag{A2}$$

and taking $\partial S_{P_0'}$ to the rhs, we obtain an eigenvalue equation for $\partial T|_{P_0}$,

$$\partial T|_{P_0} \partial S^{-1}|_{P_1} \mathbf{r}_S = \lambda_S [\partial S|_{P_0'}]^{-1} \mathbf{r}_S = \lambda_S \partial S^{-1}|_{SP_0'} \mathbf{r}_S \tag{A3}$$

where in the last step we used

$$\partial S^{-1}|_P = [\partial S|_{S^{-1}P}]^{-1} \tag{A4}$$

(A4) can be easily obtained by taking the Jacobian of $S \circ S^{-1}(P) = P$. From Eqs. (A1) and (A3) we see that ∂T and ∂T^S have the same eigenvalues at P_0 and P_1', respectively, whenever

$$\partial S^{-1}|_{P_1} = \partial S^{-1}|_{P_1'} \tag{A5}$$

Since

$$T^S = T^{-1} \qquad \text{and} \qquad \partial T^{-1}|_{P_1} = [\partial T|_{P_1'}]^{-1}$$

we conclude that ∂T has inverse eigenvalues at P_0 and P_1'. The condition (A5) is satisfied, for instance, if the Jacobian of S is constant or if the point P_1 is a fixed point ($P_1 = P_1'$).

In the following we show that the fixed points of the ABC map are grouped in pairs with inverse eigenvalues. Let us denote

$$G_1 = B \cos x; \qquad G_2 = C \cos y; \qquad G_3 = A \cos z \tag{A6}$$

Then the eigenvalues of ∂T_{ABC} at the fixed points satisfy

$$\lambda^3 - \lambda^2(G_1G_2G_3 + G_1^2 + G_2^2 + G_3^2 + 3) + \lambda(G_1^2 + G_2^2 + G_3^2 + 3 - G_1G_2G_3) - 1 = 0 \tag{A7}$$

It is easy to check that when the sign of $G_1G_2G_3$ is inverted, Eq. (A7) becomes the equation for the inverse eigenvalue $1/\lambda$. Sign reversal for $G_1G_2G_3$ can be obtained by a sign change of either one or all three G_i. As is obvious from Eq. (2.12), this only changes one fixed point into another. Therefore, for each fixed point there is another fixed point with inverse eigenvalues. Moreover, the eight fixed points can be classified into two groups of four according to $s_G = \text{sign}(G_1G_2G_3)$. Only fixed points from opposite groups collide.

APPENDIX B

Let us prove that in general a trajectory of the map cannot cross an invariant surface. Suppose there is a point P_1 below the invariant plane Σ for which $T(P_1)$ is also below Σ. Moreover, suppose that, in contradiction with the statement we want to prove, there is another point P_2 below Σ for which $T(P_2)$ is above Σ. Therefore, by continuity, there exists a point P^* lying on the straight line that connects P_1 with P_2 for which $T(P^*) \in \Sigma$ (see Fig. 13). However, this contradicts the fact that Σ is invariant, because $P^* \notin \Sigma$. The contradiction implies that either there are no points of type P_1 or none of type P_2. But any fixed point is of type P_1. Since generically there are fixed points for the integrable case somewhere in parameter space, by continuity we always have points of type P_1. Therefore, there are no crossings of invariant planes and whenever those survive in the non-integrable regime one can be sure that there is no Arnold diffusion.

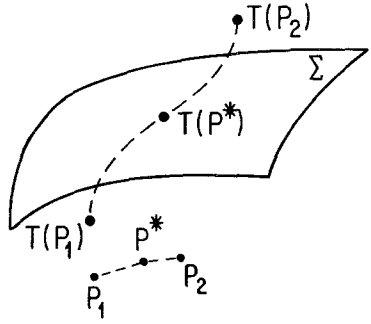

Fig. 13. Trajectories of maps cannot cross invariant surfaces.

APPENDIX C

In this appendix our aim is to derive a criterion for the onset of chaos using a Chirikov resonance overlap argument. We first estimate the size (in z) of the $(0, 1, 0)$ resonance by calculating the distance between its separatrices. For simplicity, the oscillation of the tube is neglected. Therefore, we use Eq. (3.9) to calculate on the $x = 0$ plane the distance Δ from the $z = \pi$ y-tube center to the last intersecting invariant planes. Using the notation $z_1 = \pi + \Delta$, $z_2 = \pi - \Delta$, we look for the maximal Δ for which

$$z_1 + \varepsilon H(x, 0) = z_2 + \varepsilon H(x, 0) \tag{C1}$$

After some straightforward algebra the equation

$$\sin x = \frac{\Delta}{\varepsilon \alpha_B} \frac{1 - \cos(A \sin \Delta)}{\sin(A \sin \Delta)} \tag{C2}$$

is obtained. Whenever the rhs is smaller than one, there is some x for which (C2) has a solution. Therefore, the maximal value of Δ, Δ_m, is obtained when the rhs of (C2) is equal to 1. In the limit $\Delta \to 0$, the solution to (C2) is easily obtained,

$$\Delta_m = (2\varepsilon \alpha_B / A)^{1/2} \tag{C3}$$

From Eq. (C3) we see that the approximation $\Delta \to 0$ is good whenever $B \ll A$. The width Δ_z of the resonance is related to Δ_m, and a lengthy but straightforward calculation gives $\Delta_z \approx \frac{3}{2}\Delta_m$. The overlap of the $(0, 1, 0)$ and $(0, -1, 0)$ resonances on the $x = 0$ plane will happen when $\Delta_z \approx \pi/4$. This will be used as an approximate criterion for the onset of chaos.

ACKNOWLEDGMENTS

We thank D. P. Arovas, U. Frisch, S. A. Orzag, Y. Pomeau, I. Procaccia, P. G. Saffman, and M. Tabor for useful discussions. This work was supported in part by NSF-DMR under grant 85-19460. M. F. acknowledges the support of a Dr. Chaim Weizmann Post-Doctoral Fellowship. O. P. acknowledges support by Consejo Nacional de Investigaciones Cientificas y Técnicas.

REFERENCES

1. D. J. Tritton, *Physical Fluid Dynamics* (Van Nostrand, 1977).
2. V. I. Arnold, *C. R. Acad. Sci. Paris* **261**:17 (1965).

3. M. Hénon, *C. R. Acad. Sci. Paris* **262**:312 (1966); T. Dombre, U. Frish, J. M. Greene, M. Hénon, A. Mehr, and A. M. Soward, *J. Fluid Mech.* **167**:353 (1986).
4. D. Galloway and U. Frisch, *J. Fluid Mech.*, submitted.
5. H. Aref, *J. Fluid Mech.* **143**:1 (1984); W. L. Chien, H. Rising, and J. M. Ottino, *J. Fluid Mech.* **170**:355 (1986); D. V. Khakhar, H. Rising and J. M. Ottino, *J. Fluid. Mech.* **172**:419 (1986); J. Chaiken, R. Chevray, M. Tabor, and Q. M. Tan, *Proc. R. Soc. Lond. A* **408**:165 (1986); *Phys. Fluids* **30**:687 (1987).
6. B. I. Shraiman, *Phys. Rev. A* **36**:261 (1987).
7. J. P. Gollub and T. H. Solomon, in *Proceedings of the Fritz Haber International Symposium*, I. Procaccia, ed. (Plenum Press, New York, 1987).
8. M. V. Berry, in *Topics in Nonlinear Dynamics*, S. Jorna, ed. (AIP, New York, 1978).
9. A. J. Lichtenberg and M. A. Lieberman, *Regular and Stochastic Motion* (Springer, Berlin, 1983).
10. J. M. Greene, *J. Math. Phys.* **20**:1173 (1979); S. J. Shenker and L. P. Kadanoff, *J. Stat. Phys.* **27**:631 (1981); L. P. Kadanoff, *Phys. Rev. Lett.* **47**:1641 (1981).
11. V. I. Arnold, *Dokl. Akad. Nauk SSSR* **156**:9 (1964) [*Sov. Math. Dokl.* **5**:581 (1964)]; B. V. Chirikov, *Phys. Rep.* **52**:263 (1979).
12. F. Heslot, B. Castaing, and A. Libchaber, Transition to turbulence in helium gas, preprint (1987).
13. Y. S. Sun, *Celest. Mech.* **30**:7 (1983); **33**:111 (1984).
14. A. Thyagaraja and F. A. Haas, *Phys. Fluids* **28**:1005 (1985).
15. L. Glass and R. Perez, *Phys. Rev. Lett.* **48**:1772 (1982); D. Gonzales and O. Piro, *Phys. Rev. Lett.* **50**:871 (1983).
16. G. D. Birkoff, *Dynamical Systems* (AMS, New York, 1927); V. I. Arnold and M. B. Sevryuk, in *Nonlinear Phenomena in Plasma Physics and Hydrodynamics*, R. Z. Sagdeev, ed. (MIR, Moscow, 1986).
17. G. Benettin, L. Galgani, and J.-M. Streclyn, *Phys. Rev. A* **14**:2338 (1976).